Parameters optimization of bilayer CIGS solar cell based on SCAPS-1D

Xiaotian Hua*

Department of Mechanical and Aerospace Engineering, University of California, San Diego, USA

*Corresponding author: x1hua@eng.ucsd.edu

Abstract. In this paper, numerical simulation of bilayer CIGS ($Cu(In_{1-x},a_x)Se_2$) solar cell is presented based on the codes SCAPS-1D. Specifically, the effects of Ga composition, thickness, and doping concentration on bilayer CIGS performance are investigated. In addition, this paper also discusses the interactions between some of the correlated parameters. According to the simulations, the optimized structure with 0.4 μm and 2.5 μm absorber layers achieved an efficiency of 36.16%. These results pave a path for promoting the performance of CIGS.

Keywords: CIGS solar cells, SCAPS-1D, bilayer structure, parameters optimization.

1. Introduction

CIGS solar cells are attracting extensive attention both in the laboratory and industry on account of the remarkable efficiency/cost ratio and some great properties (e.g., flexibility) [1, 2]. The efficiency of CIGS solar cells has achieved 20.8% on the polyimide substrate, and 22.8% on the glass substrate [3, 4]. Besides, some researchers focused on building bilayer or multilayer CIGS solar cells are reported to achieve higher efficiency [5, 6]. On this basis, plenty of numerical simulations were presented in current researches [6-9]. To investigate the performance of CIGS, a large range of parameters are considered in the state-of-art experimental or simulation approaches [7, 8, 10, 11].

In this study, SCAPS-1D is selected to build the model and execute the numerical simulation. The purpose of this simulation is to figure out the impacts of doping concentration, thickness, and GGI (Ga/(Ga+In)) on the bilayer CIGS structure. For the first step, a typical CIGS solar cell with a ZnO/CdS/CIGS structure was built as the default model. Subsequently, the CIGS layer is divided into two parts, and figure out the optimal parameters of bilayer CIGS. Although the thickness and doping concentration have been discussed in several research, the functions of every layer on bilayer CIGS solar cells still have little discussion which remains unclear from some perspectives. Besides, the interactions between doping concentration and thickness are also worthy to study.

The other parts of the paper are arranged as follows. The Sec. 2 will provide the main equations and data used in the simulation process. The Sec. 3 will discuss the simulation results in the modulation of parameters. Eventually, a brief summary will be given in the Sec. 4.

2.1. Simulation setups

The CIGS model is presented in Figure 1. The bandgap and electron affinity are determined by the Ga composition in $Cu(In_{1-x},a_x)Se_2$ as below [12]:

$$E_g = 1.06 + 0.39238x + 0.24762x^2 \quad (1)$$

$$\chi = 4.6 - 1.15667x + 0.03333x^2 \quad (2)$$

The simulation parameters of the CIGS model are recorded in Table 1. The simulation is processed by SCAPS-1D [13, 14]. In the simulation study, Poisson's equation is used to describe the change of electric field

$$\frac{d^2E}{dx^2} = \frac{e}{\varepsilon\varepsilon_0}\left[N_D + p + \rho_p - N_A - n - \rho_n\right] \quad (3)$$

where e denotes the electrical charge, ε and ε_0 represent the dielectric constant and the vacuum permittivity, n and p denote the electron and hole concentrations, N_A and N_D represent the acceptor and donor densities, ρ_n and ρ_p denote the trapped electron and hole concentrations. The

continuity equation of free holes and free electrons defining the carrier transport, recombination, and generation is:

$$\frac{1}{q}\frac{dJ_h}{dx} - \frac{dp}{dt} - \frac{d\rho_p}{dt} = \frac{1}{q}G - \frac{1}{q}R \quad (4)$$

$$\frac{1}{q}\frac{dJ_e}{dx} - \frac{dn}{dt} - \frac{d\rho_n}{dt} = \frac{1}{q}G - \frac{1}{q}R \quad (5)$$

where J_e and J_h represent the electron and hole current densities, R and G denote the charge recombination rate and the charge generation rate. The major carriers recombination model is SRH (Shockley-Read-Hall) recombination.

In this paper, the data of the solar spectrum of AM1.5G is referred from NREL [15]. The absorption coefficient of Al: ZnO is referred from Mamat et al.'s experiment [16]. Other electronic parameters are retrieved from several experimental and simulation results [4, 17, 18].

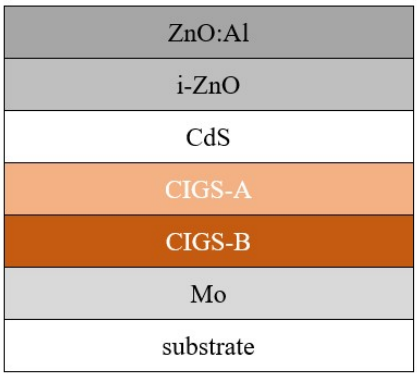

Figure. 1. Schematic diagram of bilayer CIGS.

Table.1. Physical variables for numerical simulations [17, 18].

	Al: ZnO	i-ZnO	CdS	CIGS-A	CIGS-B
W (nm)	200	100	50	1000	1500
E_g (eV)	3.3	3.3	2.4	Variable	Variable
χ (eV)	4.55	4.55	4.55	Variable	Variable
ε_r	9	9	10	13.6	13.6
N_v (1/cm^3)	1.8×10^{19}	1.8×10^{19}	9.1×10^{18}	2.2×10^{18}	2.2×10^{18}
N_c (1/cm^3)	2.2×10^{18}	2.2×10^{18}	3.1×10^{18}	2.2×10^{18}	2.2×10^{18}
ν_e (cm/s)	2.4×10^{7}	2.4×10^{7}	3.1×10^{7}	3.9×10^{7}	3.9×10^{7}
ν_h (cm/s)	1.3×10^{7}	1.3×10^{7}	1.6×10^{7}	1.4×10^{7}	1.4×10^{7}
μ_e (cm^2/(V·s))	100	100	72	100	100
μ_h (cm^2/(V·s))	31	31	20	12.5	12.5
Doping (1/cm^3)	1×10^{20}		5×10^{17}	1×10^{17}	1×10^{17}
N_t (1/cm^3)	1×10^{17}	1×10^{17}	1×10^{18}	1×10^{14}	1×10^{14}
S_e (cm^2)	1×10^{-12}	1×10^{-12}	1×10^{-17}	1×10^{-13}	1×10^{-13}
S_h (cm^2)	1×10^{-15}	1×10^{-15}	1×10^{-12}	1×10^{-14}	1×10^{-14}

2. Results & Discussion

This part will discuss the effects of the absorber layer, window layer, and buffer layer in turn. Considering the interactions between CIGS-A and CIGS-B, these two layers are discussed together about the influence of Ga composition, doping, and thickness.

2.2. Absorber layer

We selected 0, 0.31, 0.45, 0.66, and 1 as the GGI used in the simulation work. Figure 2(a) presents the V_{oc} improves with the Ga composition increasing in the CIGS-A layer. But the GGI-B, i.e. GGI in the CIGS-B layer, has little contribution to V_{oc}. Figure 2(b) illustrates combining low GGI-A and

high GGI-B promote the generation of current. It points out that the narrow bandgap in the upper layer and wide bandgap in the lower layer are more efficient for absorbing solar energy and exciting more carriers. The FF follows a similar rule to the J_{sc} in Figure 2(c), the FF can stay above about 70% when GGI-A is smaller than 0.45 and GGI-B is larger than 0.31.

Based on the trends of FF and J_{sc}, the ideal result would be a low GGI-A and high GGI-B. Because of the feature of V_{oc}, the optimal result will turn to the right side shown in Figure 2(d). The optimal parameter of GGI, 0.66 in CIGS-A and 1 in CIGS-B, will be used in our next simulation work. The result has good agreement with other simulation research in [6]. However, the role of the bottom layer of CIGS is more important in Atourki's research, attributed to differences in parameter selection (e.g., the default thickness of each layer).

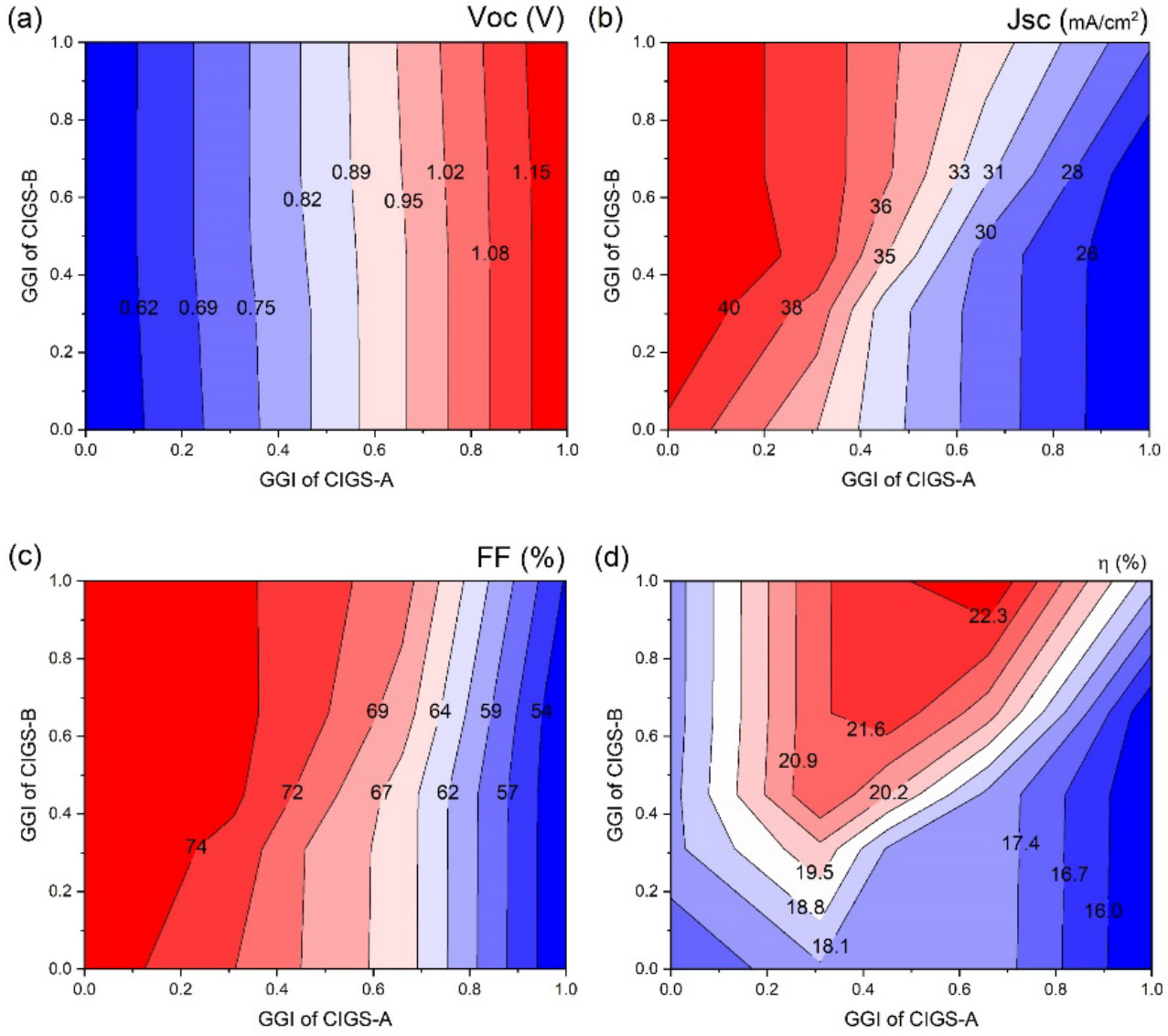

Figure. 2: (a) V_{oc} (V), (b) J_{sc} (mA/cm^2), (c) FF (%), and (d) η (%) of CIGS with the modulation of GGI in CIGS-A and CIGS-B.

The typical absorber layer of CIGS solar cells has 1.5~3 μm thickness, this simulation is also in this range. The CIGS-A has a thickness between 0.1~1.0 μm, and the CIGS-B has a thickness between 0.1~2.8 μm. The thickness of CIGS-A dominates the change of V_{oc} , but the variation is less than 5%. It means that other parameters would play a more important role in efficiency improvement. Seen from Figure 3(b), the effect of CIGS-B thickness on J_{sc} is smaller and smaller with CIGS-A thickening. It might be explained that the CIGS-A hinders the diffusion of carriers from SCR (space

charge region) to CIGS-B. Figure 3(c) illustrates that FF is capable to be higher than 80% when the thickness of CIGS-A is smaller than 0.3 μm. Thus, the efficiency can reach 26.11%by setting the thickness of CIGS-A in 0.4 μm and CIGS-B in 2.8 μm.

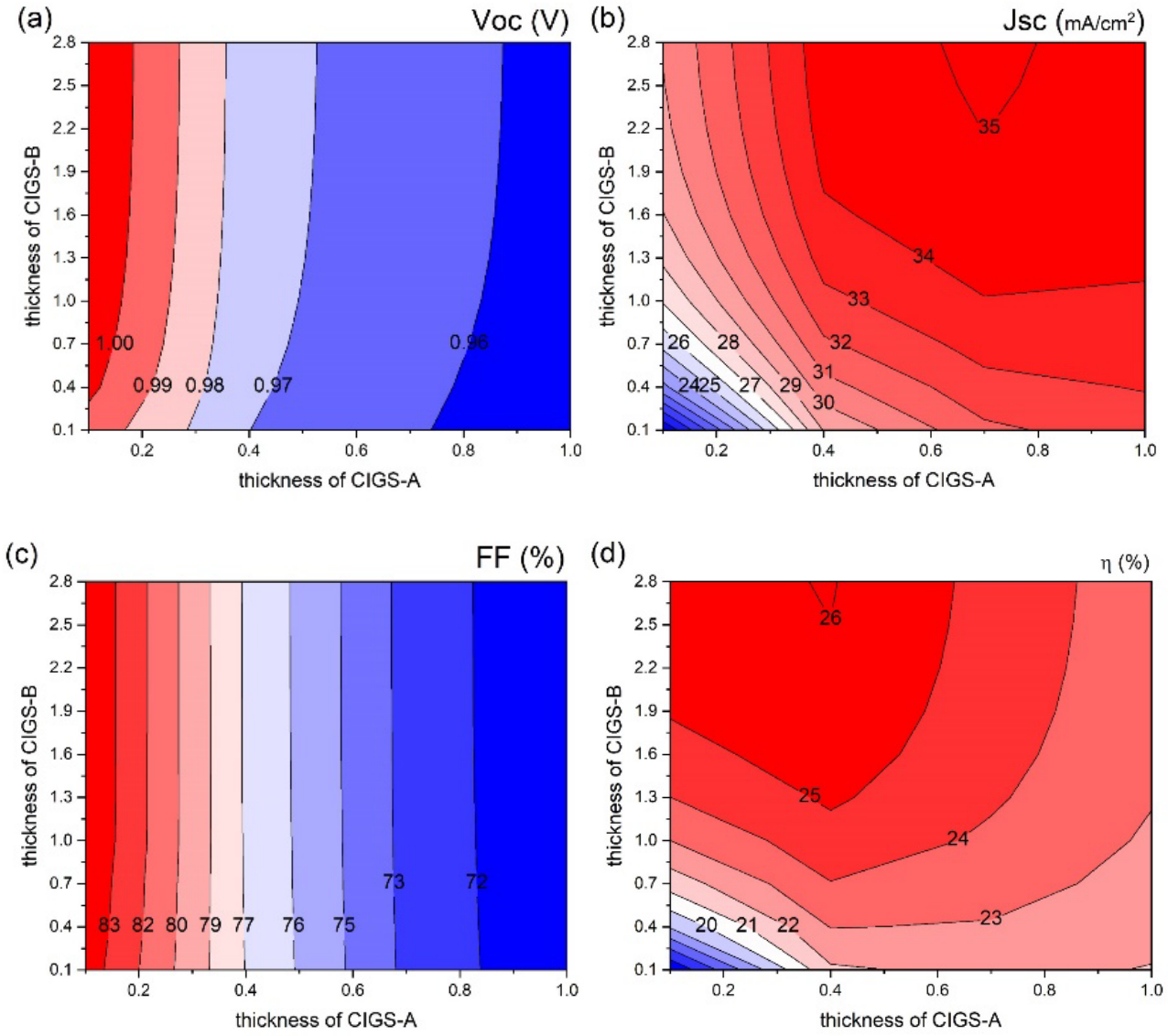

Figure. 3: (a) V_{oc} (V), (b) J_{sc} (mA/cm^2), (c) FF (%), and (d) η (%) of CIGS with the modulation of thickness in CIGS-A and CIGS-B.

The doping concentration of the CIGS-A and the CIGS-B are adjusted ranging from 10^{15}~10^{19} cm^{-3}. Compared with CIGS-B, both the V_{oc} and FF are mainly controlled by CIGS-A (seen from Figure. 4(a) and (c)). However, the J_{sc} does not follow this regulation. It is important for high J_{sc} that keeps the doping concentration of CIGS-B larger than CIGS-A as illustrated in Figure 4(c). The result in Figure 4(d) suggests that both the higher the doping concentration of CIGS-A and CIGS-B, the greater the efficiency. If the doping concentration of the CIGS-A is not more than 10^{17} cm^{-3}, CIGS-B can hardly influence the efficiency.

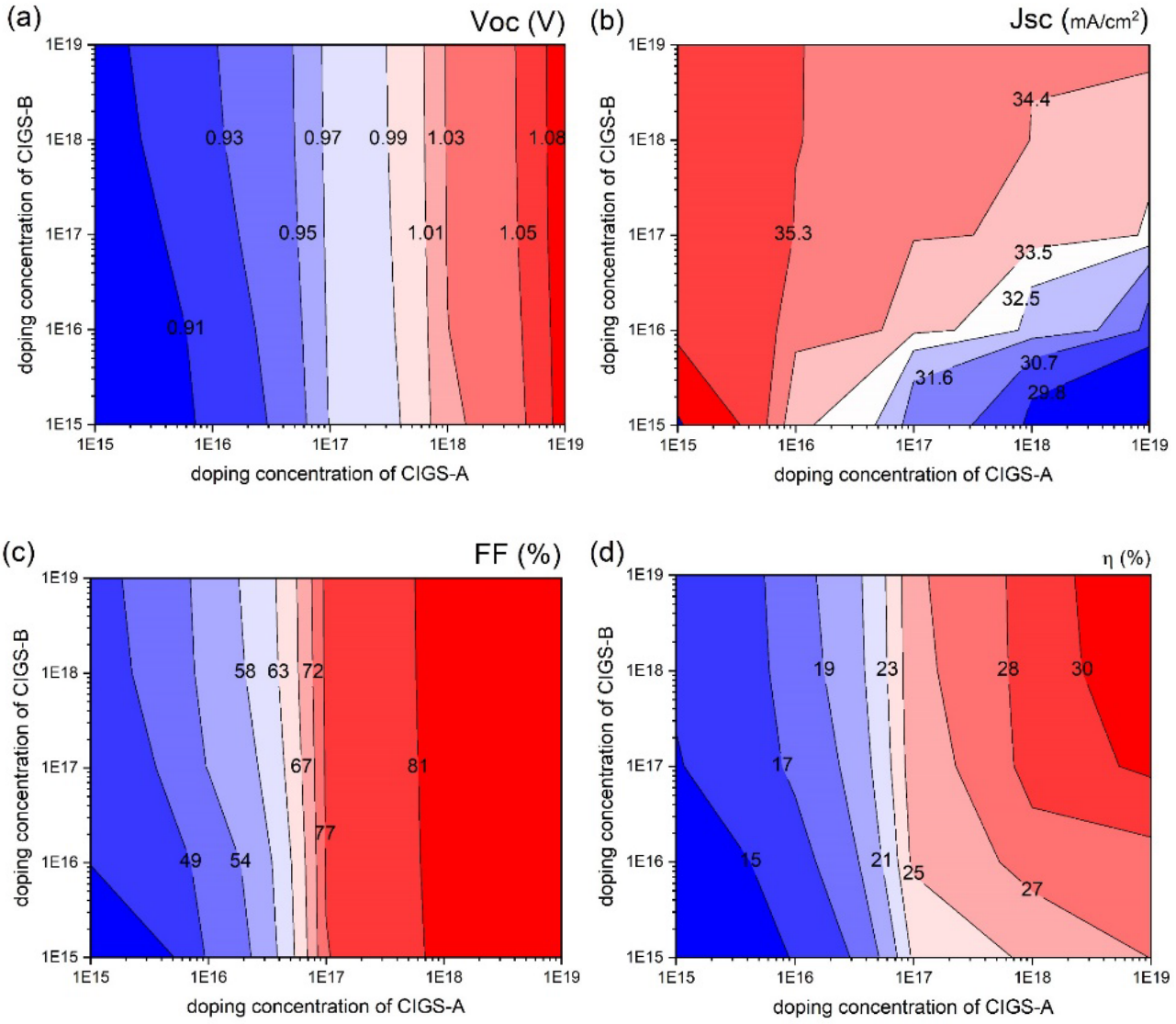

Figure. 4: (a) V_{oc} (V), (b) J_{sc} (mA/cm^2), (c) FF (%), and (d) η (%) of CIGS with the modulation of doping concentration (1/cm^3) in CIGS-A and CIGS-B.

2.3. Window layer

In this part of the simulation study, the thickness of Al: ZnO has modulated in the range of 200~20 nm. Figure 5(a) and Figure 5(b) show the J_{sc} is monotonically increasing with the decreasing thickness of Al: ZnO. The V_{oc} and FF are almost constant. Because of a thin Al: ZnO layer allows more photons to penetrate and generate electron-hole pairs, which leads to higher current density. Therefore, the 20 nm thickness is capable to achieve the highest efficiency.

Figure 5(c) and Figure 5(d) show the effect of doping concentration ranging from 10^{17} to 10^{20} cm^{-3}. According to the results, it has the stable high performance when the doping concentration reaches 10^{18} cm^{-3}. The carrier concentration is in saturation since 10^{18} cm^{-3}, hence, the window layer cannot collect more carriers with doping.

The i-ZnO layer has similar results as the Al: ZnO layer ranging 20~100 nm. With the reduction of thickness, J_{sc} enhanced, but the V_{oc} and FF are nearly unchanging in Figure 6(a) and Figure 6(b). The thickness of i-ZnO is also taken as 20 nm. However, it should be noted that, the efficiency promotes from 33.75% to 33.97% which is not significant. Some studies also have the similar results [10, 11].

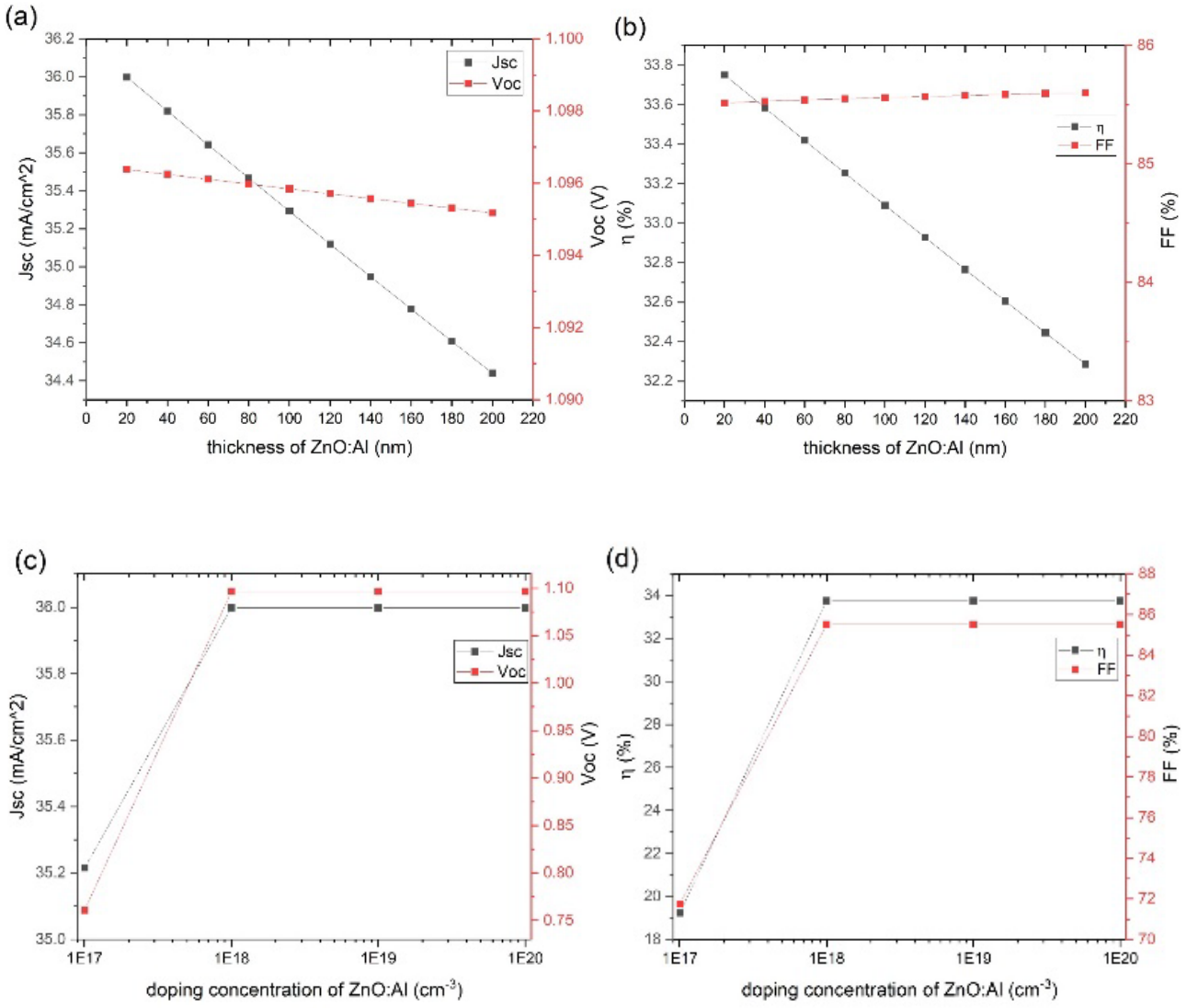

Figure. 5. The effect of modulating the thickness and the doping concentration of i-ZnO. (a) V_{oc} (V) and J_{sc} (mA/cm^2) versus thickness. (b) FF (%) and η (%) versus thickness. (c) V_{oc} (V) and J_{sc} (mA/cm^2) versus doping concentration. (d) FF (%) and η (%) versus doping concentration.

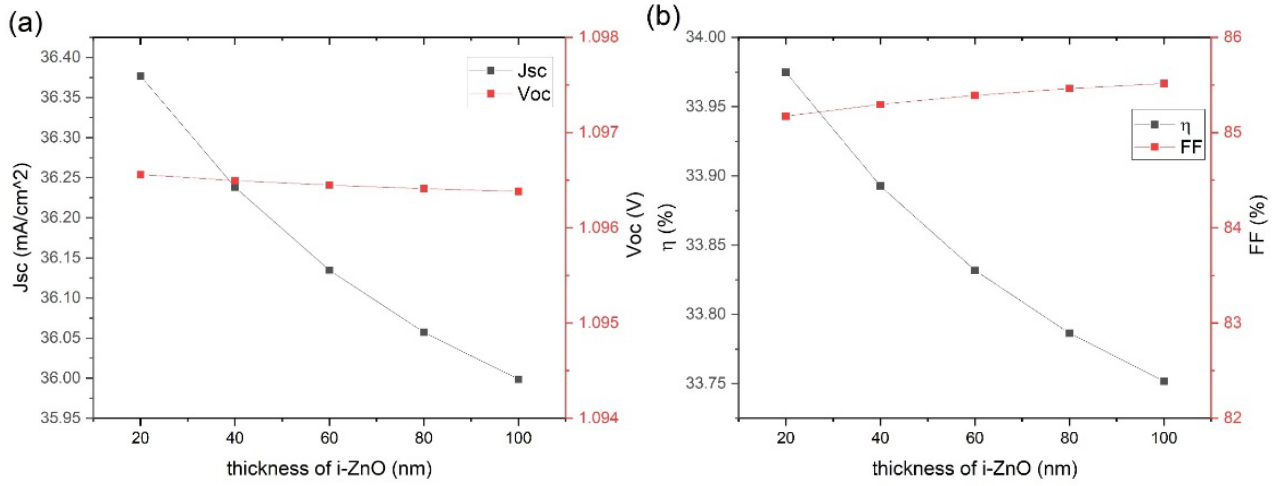

Figure. 6. The influence of modulating the thickness of i-ZnO. (a) V_{oc} (V) and J_{sc} (mA/cm^2) versus thickness. (b) FF (%) and η (%) versus thickness.

2.4. Buffer layer

The simulations parameters cover the range of CdS thickness from 50nm to 10 nm and doping concentration from 5×10^{17} to 10^{19} cm^{-3}. As can be seen from Figure 7(a), both the doping concentration and thickness affect V_{oc} limited. Following the doping concentration rising, J_{sc} decreases and FF increases slightly between 10~50 nm as illustrated in Figure 7(b) and Figure 7(c). Interestingly, the efficiency was observed the effect of doping concentration is not obvious, the effect of doping on J_{sc} and FF cancel each other out. The result suggests that diminishing the thickness of CdS makes superior efficiency, and the effect of doping concentration from 5×10^{17} to 10^{19} cm^{-3} is small.

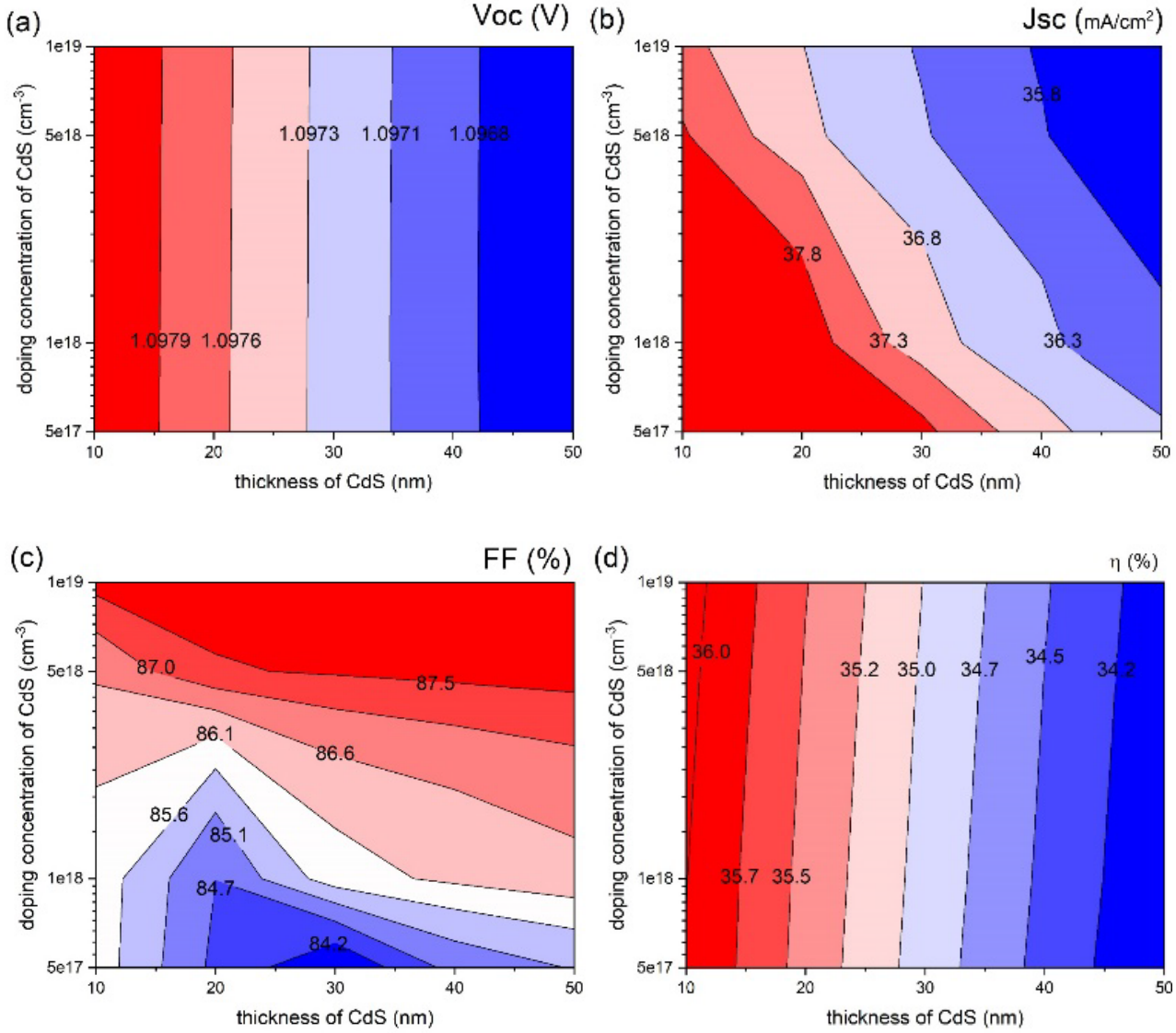

Figure. 7. (a) V_{oc} (V), (b) J_{sc} (mA/cm^2), (c) FF (%), and (d) η (%) of CIGS with the modulation of doping concentration and thickness in CdS.

2.5. Optimal structure

According to the simulation work above, GGI, thickness and doping concentration are discussed for optimization. There is an impressive increase in V_{oc} from 0.73 V to 1.10 V, which benefits from the selection of GGI in the CIGS layer. As the data recorded in Table 2 and the J-V curves in Figure 8, the efficiency promotes from 20.07% to 36.16%. The result is similar to Ghavami et al.'s simulation research of bilayer CIGS solar cell [9].

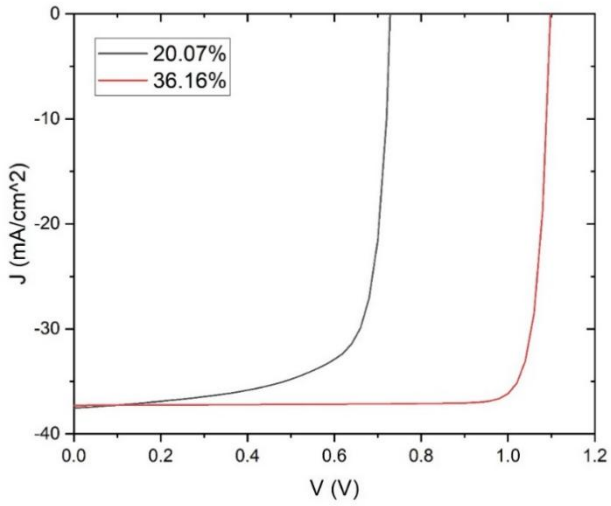

Figure. 8. J-V curves comparison of CIGS. The black line is the initial result. The red line is the optimal result.

Table.2. Performance parameters before and after optimization.

Parameters	V_{oc} (V)	J_{sc} (mA/cm^{-3})	FF (%)	η (%)
before	0.73	37.55	73.49	20.07
after	1.10	37.27	88.35	36.16

2.6. Limitation

There are several possible limitations and defects in this study. The first one is the sampling density might be not enough, which might miss the optimal result. When calculating the effect of Ga composition, only 5 points are selected for each layer, which may lead to the shifting of the optimal result. Another limitation is the range applied in this simulation study. A suitable range can control the amount of calculation and provide a more obvious correlation assisting analysis. Achieving higher accuracy with lower amount of calculation is also the direction of effort.

3. Conclusions

To sum up, this study discussed the effects of several parameters on the bilayer CIGS based on the SCAPS-1D. The interaction between two CIGS layers is mentioned. According to the results, the increase of V_{oc} close to 50% is the main reason for efficiency rising from 20.07% to 36.16%. Further researches ought to focus on the characteristics of multi-graded CIGS solar cells. In the future, modulating the bandgap more specifically would be a promising way to improve performance. Overall, these results offer a guideline for modulating the performance of bilayer CIGS.

References

[1] Ramanujam J, Bishop D M, Todorov T K, et al. Flexible CIGS, CdTe and a-Si: H based thin film solar cells: A review[J]. Progress in Materials Science, 2020, 110: 100619.

[2] Kaelin M, Rudmann D, Tiwari A N. Low cost processing of CIGS thin film solar cells[J]. Solar Energy, 2004, 77(6): 749-756.

[3] Carron R, Nishiwaki S, Feurer T, et al. Advanced alkali treatments for high-efficiency Cu (In, Ga) Se2 solar cells on flexible substrates[J]. Advanced Energy Materials, 2019, 9(24): 1900408.

[4] Kamada R, Yagioka T, Adachi S, et al. New world record Cu (In, Ga)(Se, S) 2 thin film solar cell efficiency beyond 22%[C]//2016 IEEE 43rd Photovoltaic Specialists Conference (PVSC). IEEE, 2016: 1287-1291.

[5] Noikaew B, Sukaiem S, Namnuan B, et al. CIGS thin film solar cells with graded-band gap fabricated by CIS/CGS bilayer and CGS/CIS/CGS trilayer systems[C]//Journal of Physics: Conference Series. IOP Publishing, 2018, 1144(1): 012069.

[6] Atourki L, Kirou H, Ihlal A, et al. Numerical study of thin films CIGS bilayer solar cells using SCAPS[J]. Materials Today: Proceedings, 2016, 3(7): 2570-2577.

[7] Heriche H, Rouabah Z, Bouarissa N. New ultra thin CIGS structure solar cells using SCAPS simulation program[J]. International Journal of Hydrogen Energy, 2017, 42(15): 9524-9532.

[8] Liu W, Li H, Qiao B, et al. Highly efficient CIGS solar cells based on a new CIGS bandgap gradient design characterized by numerical simulation[J]. Solar Energy, 2022, 233: 337-344.

[9] Ghavami F, Salehi A. High-efficiency CIGS solar cell by optimization of doping concentration, thickness and energy band gap[J]. Modern Physics Letters B, 2020, 34(04): 2050053.

[10] Dabbabi S, Nasr T B, Kamoun-Turki N. Parameters optimization of CIGS solar cell using 2D physical modeling[J]. Results in physics, 2017, 7: 4020-4024.

[11] Movla H. Optimization of the CIGS based thin film solar cells: Numerical simulation and analysis[J]. Optik, 2014, 125(1): 67-70.

[12] Nya F T, Kenfack G M D. Thin-Film Solar Cells Performances Optimization: Case of Cu (In, Ga) Se2-ZnS[J]. Solar Cells: Theory, Materials and Recent Advances, 2021: 85.

[13] Burgelman M, Nollet P, Degrave S. Modelling polycrystalline semiconductor solar cells[J]. Thin solid films, 2000, 361: 527-532.

[14] Burgelman M, Decock K, Khelifi S, et al. Advanced electrical simulation of thin film solar cells[J]. Thin Solid Films, 2013, 535: 296-301.

[15] Collins D G, Blättner W G, Wells M B, et al. Backward Monte Carlo calculations of the polarization characteristics of the radiation emerging from spherical-shell atmospheres[J]. Applied Optics, 1972, 11(11): 2684-2696.

[16] Mamat M H, Sahdan M Z, Amizam S, et al. Optical and electrical properties of aluminum doped zinc oxide thin films at various doping concentrations[J]. Journal of the ceramic society of Japan, 2009, 117(1371): 1263-1267.

[17] Liu Y, Li B, Lin S, et al. Numerical analysis on effects of experimental Ga grading on Cu (In, Ga) Se2 solar cell performance[J]. Journal of Physics and Chemistry of Solids, 2018, 120: 190-196.

[18] Ouédraogo S, Zougmoré F, Ndjaka J M. Numerical analysis of copper-indium-gallium-diselenide-based solar cells by SCAPS-1D[J]. International Journal of photoenergy, 2013, 2013.